PHYSICAL REVIEW D **83,** 083507 (2011)

Photon spectra from WIMP annihilation

J. A. R. Cembranos,[1,2,*] A. de la Cruz-Dombriz,[2,†] A. Dobado,[2,‡] R. A. Lineros,[3,§] and A. L. Maroto[2,‖]

[1]*William I. Fine Theoretical Physics Institute, University of Minnesota, Minneapolis, Minnesota 55455, USA and School of Physics and Astronomy, University of Minnesota, Minneapolis, Minnesota 55455, USA*

[2]*Departamento de Física Teórica I, Universidad Complutense de Madrid, E-28040 Madrid, Spain*

[3]*INFN sezione di Torino, I-10122 Torino, Italy and Dipartimento di Fisica Teorica, Università di Torino, I-10122 Torino, Italy*

(Received 15 October 2010; published 11 April 2011)

If the present dark matter in the Universe annihilates into standard model particles, it must contribute to the fluxes of cosmic rays that are detected on the Earth and, in particular, to the observed gamma-ray fluxes. The magnitude of such a contribution depends on the particular dark matter candidate, but certain features of the produced photon spectra may be analyzed in a rather model-independent fashion. In this work we provide the complete photon spectra coming from WIMP annihilation into standard model particle-antiparticle pairs obtained by extensive Monte Carlo simulations. We present results for each individual annihilation channel and provide analytical fitting formulas for the different spectra for a wide range of WIMP masses.

DOI: 10.1103/PhysRevD.83.083507 PACS numbers: 95.35.+d, 98.80.Cq

I. INTRODUCTION

According to present observations of large scale structures, cosmic microwave background anisotropies and light nuclei abundances, the most important component of matter in the Universe cannot be accommodated within the standard model (SM) of elementary particles. Indeed, dark matter (DM) cannot be made of any of the known particles, and this is one of the most appealing arguments for the existence of new physics. Indeed DM is a required component not only on cosmological scales, but also for a satisfactory description of rotational speeds of galaxies, orbital velocities of galaxies in clusters, gravitational lensing of background objects by galaxy clusters, such as the bullet cluster, and the temperature distribution of hot gas in galaxies and clusters of galaxies. The experimental determination of the DM nature will require the interplay of collider experiments [1] and astrophysical observations. These searches use to be classified in direct or indirect searches (see [2,3] for different alternatives). Nevertheless, nongravitational evidence of its existence and a concrete understanding of its nature still remain elusive. Concerning direct searches, the elastic scattering of DM particles from nuclei should lead directly to observable nuclear recoil signatures. Although the number of DM particles which passes through the Earth each second is quite large, the weak interactions between DM and the standard matter make DM direct detection extremely difficult.

On the other hand, DM might be detected indirectly, by observing their annihilation products into SM particles. Thus, even if weakly interacting massive particles (WIMPs) are stable, two of them may annihilate into ordinary matter such as quarks, leptons and gauge bosons. Their annihilation in different places (galactic halo, Sun, Earth, etc.) produce cosmic rays to be discriminated through distinctive signatures from the background. After WIMPs annihilation a cascade process would occur. In the end the potentially observable stable particles would be neutrinos, gamma rays, positrons, and antimatter (antiprotons, antihelium, antideuterions, etc.), which may be observed through different devices. Neutrinos and gamma rays have the advantage of maintaining their original direction thanks to their null electric charges. On the contrary, charged particles' searches, such as those of positrons and other antimatter particles, are hindered by propagation trajectories.

The detection of such indirect signals would not constitute conclusive evidence for DM since the uncertainties in the specific DM interactions, DM densities, and backgrounds from other sources are not fully understood yet. Nevertheless, this work precisely focuses on this kind of detection as an indirect method to get information about the DM nature, abundance, and properties.

Photon fluxes in specific DM models are usually obtained by software packages such as DARKSUSY and MICROMEGAS based on PYTHIA Monte Carlo event generator. In general, for a particular supersymmetry model and a given WIMP mass, the total photon spectrum is obtained from the addition of the contributions from different channels. In this sense, it would be interesting to have a fitting function for the shape of the spectra corresponding to each individual annihilation channel and, in addition, determine the dependence of such spectra on the WIMP mass in a model-independent way. Previous attempts of analytically capturing the photon spectra for different annihilation channels were presented in [4,5] but only for some channels and two particular WIMP masses. These efforts did

*cembranos@physics.umn.edu
†dombriz@fis.ucm.es
‡dobado@fis.ucm.es
§lineros@to.infn.it
‖maroto@fis.ucm.es

not cover the whole photon energy range since the proposed parametrization for the gamma-ray flux was given by a single exponential. More recent attempts [6] also studied two WIMP masses (500 GeV and 1 TeV) for quarks, W, Z, gluon, and τ lepton channels.

The obtained fitting function could be used to obtain photon fluxes for alternative dark matter candidates for which software packages have not been developed. On the other hand, the information about channel contribution and mass dependence can be very useful in order to identify certain gamma-ray features as signals of specific WIMP candidates.

The paper is organized as follows: in Sec. II, we briefly review the standard procedure for the calculation of gamma-ray fluxes from WIMP pair annihilations. In Sec. III, we comment on several aspects of detectors and backgrounds. Section IV is then devoted to the details of specific simulations performed with PYTHIA. In Sec. V, we introduce the fitting formulas that will be used to describe the spectra and in Sec. VI the results for the simulations, the fitted parameters, and their dependence on the WIMP mass are presented. Then, in Sec. VII we provide some information about the performed numerical codes obtained from our results and available online. Section VIII is then devoted to the main conclusions of the work. Finally, an Appendix is provided to illustrate the obtained results for some studied annihilation channels.

II. GAMMA-RAY FLUX FROM DM ANNIHILATION

Let us denote the DM mass by M and its thermal averaged annihilation cross section into two SM particles (labeled by the subindex i) by $\langle \sigma_i v \rangle$. Then the γ-ray flux from all possible annihilation channels is given by

$$\frac{d\Phi_\gamma^{\mathrm{DM}}}{dE_\gamma} = \underbrace{\frac{1}{4\pi M^2}\sum_i \langle \sigma_i v \rangle \frac{dN_\gamma^i}{dE_\gamma}}_{\text{Particle model dependent}} \times \underbrace{\frac{1}{\Delta\Omega}\int_{\Delta\Omega} d\Omega \int_{\text{l.o.s.}} \rho^2[r(s)]ds,}_{\text{Dark matter density dependent}} \quad (1)$$

where ρ is the DM density as a function of distance from its center r, which depends on the heliocentric distance s. The integral is performed along the line-of-sight (l.o.s.) to the target and averaged over the detector solid angle $\Delta\Omega$.

The first piece of the right-hand side in (1) depends on the particular particle physics model for DM annihilations. In particular, the self-annihilation cross sections are mainly described by the theory explaining the WIMP physics, whereas the number of photons produced in each decaying channel per energy interval involves decays and/or hadronization of unstable products, for instance quarks and gauge bosons. Consequently, the detailed study of these decay chains and nonperturbative effects related to QCD is a hard task to be accomplished by any analytical approach. The second piece in (1) is a line-of-sight integration through the DM density distribution. We will discuss each of these pieces separately.

A. Particle physics model

Although annihilation cross sections are not known, they are restricted by collider constraints and direct detection. In addition, the thermal relic density in the range $\Omega_{\mathrm{CDM}}h^2 = 0.1123 \pm 0.0035$ which is determined by fitting the standard ΛCDM model to the WMAP7 data (Wilkinson Microwave Anisotropy Probe results for 7 years of observations) [7], the latest measurements from the Baryon acoustic oscillations in the distribution of galaxies [8] and the Hubble constant (H_0) measurement [9], does not allow an arbitrary contribution from the DM gamma-ray fluxes.

As already mentioned, the annihilation of WIMPs is closely related to SM particle production. The time scale of an annihilation process is shorter than typical astrophysical scales. This fact implies that only stable or very long-lived particles survive to the WIMP annihilations and may therefore be observed by detectors.

For most of the DM candidates, the production of monoenergetic photons is very suppressed. The main reason for such a suppression comes from the fact that DM is neutral. Thus, it is usually assumed that the gamma-ray signal comes fundamentally from secondary photons originated in the cascade of decays of gauge bosons and jets produced from WIMP annihilations. These annihilations would produce in the end a broad energy distribution of photons, which would be difficult to be distinguished from the background. However, the directional dependence of the gamma-ray intensity coming from these annihilations is mainly localized in pointlike sources as will be discussed in the following section. This fact could therefore provide a distinctive signature.

In conclusion, for a particular DM candidate, a unique annihilation channel may dominate, but in general, they all contribute. All those channels contributions produce a broad energy gamma-ray flux, whose maximum constitutes a potential signature for its detection. Typically, this peak is centered at an energy that is 1 order of magnitude lower than the mass of the DM candidate.

On the other hand, a different strategy can be followed by taking into account the fact that the cosmic-ray background is suppressed at high energies. Primary photons coming from the Weicksäcker-Williams radiation dominate the spectrum at energies close to the mass of the DM candidate and their signature is potentially observable as a cutoff [10]. This approach has the advantage of being less sensitive to electroweak corrections which may be important if the mass of the DM candidate is larger than the electroweak scale [11].

B. DM density directionality

The line-of-sight integration can be obtained from

$$\langle J\rangle_{\Delta\Omega} \doteq \frac{1}{\Delta\Omega}\int_{\Delta\Omega} J(\psi)d\Omega = \frac{2\pi}{\Delta\Omega}\int_0^{\theta_{\max}} d\theta\sin\theta \times \int_{s_{\min}}^{s_{\max}} ds\rho^2(\sqrt{s^2+s_0^2-2ss_0\cos\theta}), \quad (2)$$

where

$$J(\psi) = \int_{\text{l.o.s.}} ds\rho^2(r). \quad (3)$$

The angled brackets denote the averaging over the solid angle $\Delta\Omega$, and $s_{\min}$ and $s_{\max}$ are the lower and upper limits of the line-of-sight integration: $s_0\cos\theta \pm \sqrt{r_t^2 - s_0^2\sin^2\theta}$. In this formula s_0 is the heliocentric distance and r_t is the tidal radius.

Traditionally, the Galactic center has attracted the attention of this type of directional analysis since standard cusped Navarro-Frenk-White halos predict the existence of a very important amount of DM in that direction [12]. However, this assumption is in contradiction with a substantial body of astrophysical evidences [13], and a core profile is not sensitive to standard DM candidates. On the contrary, cusped profiles are not excluded for the local group dwarf spheroidals that constitute interesting targets since they are much more dominated by DM. In this way, directional analysis towards Canis Major, Draco, and Sagittarius or Segue 1 [14] are more promising.

In any case, galaxy clusters are also promising targets [15]. Another alternative strategy takes advantage of the large field of view of FERMI, that may be sensitive to the continuum photon flux coming from DM annihilation at moderate latitudes ($|b| > 10°$) [12]. Other proposed targets, as the large magellanic cloud [16], are less interesting since their central parts are dominated by baryonic matter.

III. DETECTORS AND BACKGROUNDS

$\theta_{\max}$ in Eq. (2) is the angle over which we average, and is bounded from below by the experimental resolution of the particular detector:

$$\Delta\Omega = 2\pi\int_0^{\theta_{\max}} d\theta\sin\theta = 2\pi(1-\cos(\theta_{\max})). \quad (4)$$

The quoted point spread function widths for the various experiments are typically: 0.4° (EGRET), 0.1° (CANGAROO-III, FERMI, HESS, MAGIC, and VERITAS). EGRET and FERMI are satellite detectors with low energy thresholds (about 100 MeV), high-energy resolution ($\sim 15\%$) but only moderate angular precision. The others are atmospheric Cerenkov telescopes (ACTs) with higher thresholds (≈ 100 GeV) but better angular resolution. Typical reference sizes for the solid angle are $\Delta\Omega = 10^{-5}$ sr for ACTs and FERMI and $\Delta\Omega = 10^{-3}$ sr for EGRET. In any case, the mentioned values only illustrate the general situation, since the solid angle for each experiment depends on the energy. In particular, for FERMI, the 0.1° point spread function is only valid for energies of about 100 GeV [17].

There are different main sources of background for the signal under consideration: hadronic, cosmic-ray electrons, localized astrophysical sources, and the diffuse γ rays. The latter is negligible for ACTs, but only the last two are present for satellite experiments like FERMI or EGRET.

For heavy WIMPs, the produced high-energy gamma photons could be in the range 30 GeV–10 TeV, detectable by ACTs such as HESS, VERITAS, or MAGIC. On the contrary, for lighter WIMPs, the photon fluxes would be in the range detectable by space-based gamma-ray observatories [18] such as EGRET, FERMI, or AMS, with better sensitivities around 30 MeV–300 GeV.

IV. MONTE CARLO SPECTRA GENERATION: TECHNICALITIES

In this section, we explicitly specify how gamma rays spectra have been generated. We have used a widely known particle physics software, PYTHIA (version 6.418) [19], to obtain the results we are about to present. In a first approximation, the WIMP annihilation is described by two separated processes: The first one describes the annihilation of WIMP particles and its output which are particle-antiparticle SM pairs. The details are contained in the theory describing the WIMP physics. The second process considers the evolution (decays and/or hadronization) of the SM unstable products, for instance, quarks and gauge bosons. Unfortunately, a first-principle description of this latter step is too complex due to chain decays and nonperturbative QCD effects.

As we mentioned above, in this work we have used PYTHIA to generate the photon energy spectra starting from pairs of SM particles, where each pair respects WIMP annihilation quantum numbers like neutral charge and color singlet. As will be described below, we will allow for final state radiation from charged particles to contribute to the photon spectra. Because of the expected velocity dispersion of DM, we expect most of the annihilations to happen quasistatically. This fact offers the center of mass (CM) frame as the most suitable frame to produce the photon spectra. Hence, the process is described by the total energy:

$$E_{\text{CM}} \simeq 2M, \quad (5)$$

where M is the mass of the WIMP particle. Therefore, by considering different CM energies for the SM particles pairs in each WIMP annihilation process we are indeed studying different WIMP masses. The procedure to obtain the photon spectra is thus straightforward, except for the

particular case of the t quark. For any given pair of SM particles which are produced in the WIMP annihilation, we count the number of photons in each bin of energy and then normalize them to the total number of simulated pair collisions. The bins which we have considered in the x variable, $x \equiv E_\gamma/M$, are: $[10^{-5}, 10^{-3}]$, $[10^{-3}, 0.2]$, [0.2, 0.5], [0.5, 0.8], and [0.8, 1.0]. Nevertheless, for some studied channels more precision was needed in some particular energy intervals and additional bins were considered.

The number of required photons in each bin was fixed *a priori*. Nevertheless, this number was changed sometime in order to provide suitable statistics of produced photons. For instance, for the high-energy bins many collisions are required to get a significant number of photons, whereas for low-intermediate energy, many photons are usually produced even for a small number of collisions. The total number of photons corresponding to the different generated pairs in terms of the WIMP mass are presented in Tables I, II, and III.[1] When these results are normalized with respect to the number of WIMP annihilations, one gets the number of photons per WIMP annihilation for each channel and WIMP mass. At the end of the paper, Fig. 9 in the Appendix illustrates these results.

The SM particle pairs decays generated are W and Z gauge bosons; τ and μ leptons; and u, d, s, c, b and t quarks. For each annihilation channel we have studied the gamma-ray spectra produced for different WIMP masses. The result of the simulations were fitted to analytical expressions as is described in the following section.

TABLE I. Total number of photons—in 10^7 units—generated from W^+W^-, ZZ, and $t\bar{t}$ channels for different WIMP masses.

Channel\Mass (GeV)	100	125	150	200	250	350	500	1000
W^+W^-	5.21	⋯	1.91	6.85	⋯	7.83	2.91	2.85
ZZ	0.42	6.01	2.91	14.9	⋯	14.2	2.81	2.02
$t\bar{t}$	⋯	⋯	⋯	0.70	0.86	0.32	2.81	1.41

TABLE II. Total number of photons—in 10^7 units—generated from $\tau^+\tau^-$ and $\mu^+\mu^-$ channels for different WIMP masses. The required number of photons per bin was fixed to the same figure for both channels in each bin. This choice was statistically justified according to the obtained simulated plots.

Channel\Mass (GeV)	25	50	100	200	500	1000	10^4	5×10^4
$\tau^+\tau^-$	2.25	2.25	2.23	1.07	2.81	2.33	8.41	7.80
$\mu^+\mu^-$	2.25	2.25	2.23	1.07	2.81	2.33	8.41	7.80

TABLE III. Total number of photons—in 10^7 units—generated from $u\bar{u}$, $d\bar{d}$, $s\bar{s}$, $c\bar{c}$, and $b\bar{b}$ channels for different WIMP masses.

Channel\ Mass (GeV)	50	100	200	500	1000	2000	5000	7000	8000
$u\bar{u}$	2.05	11.9	2.42	2.81	3.82	10.8	5.91	⋯	2.11
$d\bar{d}$	1.04	1.96	2.42	2.81	2.81	2.81	2.31	⋯	⋯
$s\bar{s}$	15.3	2.00	1.97	2.81	9.82	2.71	2.71	11.0	⋯
$c\bar{c}$	2.41	1.99	16.8	2.81	2.81	3.81	12.0	⋯	3.00
$b\bar{b}$	11.7	1.91	2.62	2.61	8.81	2.20	3.81	⋯	1.70

A. Final state radiation

If the final state in the annihilation process contains charged particles, there is a finite probability of emission of an additional photon. This is discussed in detail in [20]. In principle there are two types of contributions: that coming from photons directly radiated from the external legs, which is the final state radiation we have considered in the work, and that coming from virtual particles exchanged in the WIMP annihilation process. The first kind of contribution can be described for relativistic final states by means of a universal Weizsäcker-Williams term fundamentally independent from the particle physics model [20]. On the other hand, radiation from virtual particles only takes place in certain DM models and is only relevant, in particular, cases, for instance, when the virtual particle mass is almost degenerate with the WIMP mass. Even in these cases, it has been shown [21] that although this effect has to be included for the complete evaluation of fluxes of high-energy photons from WIMP annihilation, its contribution is relevant only in models and at energies where the lines contribution is dominant over the secondary photons. For those reasons and since the aim of the present work is to provide model-independent results for photon spectra, only final state radiation was included in our simulations.

B. The case for t quark decay

The decay of top quark is not explicitly included in the PYTHIA package. We have approximated this process by its dominant SM decay, i.e., each (anti) top decays into $W^{+(-)}$ and (anti) bottom. In order to maintain any nonperturbative effect, we work on an initial four-particle state composed by W^+b coming from the top and $W^-\bar{b}$ from antitop, which keeps all kinematics and color properties from the original pair. Starting from this configuration, we have forced decays and hadronization processes to evolve as PYTHIA does and therefore, the gamma rays spectra corresponding to this channel have also been included in our analysis.

[1]The raise in the total number of photons for certain mass values in these tables is due to the fact that in order to get good enough statistics in certain channels and/or WIMP masses additional bins and computation time was required.

V. ANALYTICAL FITS TO PYTHIA SIMULATION SPECTRA

In this section we present the fitting functions used for the different channels. According to the PYTHIA simulations described in the previous section, three different parametrizations were required in order to fit all available data from the studied channels. The first one for quarks (except the top) and leptons. Then, a second one for gauge bosons W and Z and a third one for the top.

A. Quarks and leptons

For quarks (except the top), τ and μ leptons, the most general formula needed to reproduce the behavior of the differential number of photons per photon energy may be written as:

$$x^{1.5}\frac{dN_\gamma}{dx} = a_1 \exp\left(-b_1 x^{n_1} - b_2 x^{n_2} - \frac{c_1}{x^{d_1}} + \frac{c_2}{x^{d_2}}\right) + q x^{1.5} \ln[p(1-x)]\frac{x^2-2x+2}{x}. \quad (6)$$

In this formula, the logarithmic term takes into account the final state radiation through the Weizsäcker-Williams expression [20,22]. Nevertheless, initial radiation is removed from our Monte Carlo simulations in order to avoid wrongly counting their possible contributions.

Strictly speaking, the p parameter in the Weizsäcker-Williams term in the previous formula is $(M/m_{\text{particle}})^2$ where m_{particle} is the mass of the charged particle that emits radiation. However in our case, it will be a free parameter to be fitted since the radiation comes from many possible charged particles, which are produced along the decay and hadronization processes. Therefore we are encapsulating all the bremsstrahlung effects in a single Weizsäcker-Williams–like term.

Concerning the μ lepton, the expression above (6) becomes simpler since the exponential contribution is absent. The μ^- decays in $e^-\bar{\nu}_e\nu_\mu$ with a branching ratio of ~ 1 and therefore the only contribution in addition to its own bremsstrahlung, is provided by the radiation coming from the electron. The total gamma rays flux is thus well fitted by

$$x^{1.5}\frac{dN_\gamma}{dx} = q x^{1.5} \ln[p(1-x^l)]\frac{x^2-2x+2}{x}, \quad (7)$$

where the l parameter in the logarithm is needed in order to fit the simulations as will be seen in the corresponding sections.

Let us mention at this stage that for the gamma rays obtained from electron-positron pairs, the only contribution is that coming from bremsstrahlung. Therefore, the previous expression (7) is also valid with $q = \alpha_{\text{QED}}/\pi$, $p = (M/m_{e^-})^2$, and $l \equiv 1$. This choice of the parameters corresponds of course to the well-known Weizsäcker-Williams formula.

B. W and Z bosons

For the W and Z gauge bosons, the parametrization used to fit the Monte Carlo simulation is

$$x^{1.5}\frac{dN_\gamma}{dx} = a_1 \exp\left(-b_1 x^{n_1} - \frac{c_1}{x^{d_1}}\right)\left\{\frac{\ln[p(j-x)]}{\ln p}\right\}^q. \quad (8)$$

This expression differs from the expression (6) in the absence of the additive logarithmic contribution. Nonetheless, this contribution acquires a multiplicative behavior. The exponential contribution is also quite simplified with only one positive and one negative power laws. Moreover, a_1, n_1, and q parameters appear to be independent of the WIMP mass M as will be seen in the corresponding section. The rest of parameters, i.e., b_1, c_1, d_1, p, and j, are WIMP mass dependent and will be determined for each WIMP mass and for the W and Z separately. In both cases we have covered a WIMP mass range from 100 to 10^4 GeV. Nonetheless, at masses higher than 1000 GeV, we have observed no significant change in the photon spectra for both particles.

C. t quark

Finally, for the top, the required parametrization turned out to be

$$x^{1.5}\frac{dN_\gamma}{dx} = a_1 \exp\left(-b_1 x^{n_1} - \frac{c_1}{x^{d_1}} - \frac{c_2}{x^{d_2}}\right)\left\{\frac{\ln[p(1-x^l)]}{\ln p}\right\}^q. \quad (9)$$

Likewise the previous case for W and Z bosons, gamma-ray spectra parametrization for the top is quite different from that given by expression (6). This time, the exponential contribution is more complicated than the one in expression (8), with one positive and two negative power laws. Again, the additive logarithmic contribution is absent but it acquires a multiplicative behavior. Notice the exponent l in the logarithmic argument, which is required to provide correct fits for this particle.

The covered WIMP mass range for the top case was from 200 to 10^5 GeV. Nevertheless, at masses higher than 1000 GeV we have observed again that there is no significant change in the gamma-ray spectra.

VI. RESULTS FROM PYTHIA SIMULATION

In this section we present the results of our fit of the parameters given by expressions (6), (8), and (9) after having performed the PYTHIA simulations described in Sec. IV. For each studied channel, we have considered the possibility of parameters depending on the WIMP mass.

Once the parameters in expressions (6), (8), and (9) have been determined for each channel and different WIMP masses, it is possible to study their evolution with the WIMP mass M. Some parameters in expressions are WIMP mass independent and take values that depend on the studied channel. The rest are WIMP mass dependent.

TABLE IV. *W boson*: b_1, c_1, d_1, p, and j parameters corresponding to (8) in the W^+W^- channel for different WIMP masses. Mass independent parameters in (8) for this channel are presented at the bottom of the table.

WIMP mass (GeV)	b_1	c_1	d_1	p	j
100	9.48	0.651	0.292	973	0.790
150	8.87	0.808	0.261	783	0.919
200	8.64	0.882	0.250	684	0.955
350	8.56	0.907	0.245	593	0.991
500	8.51	0.917	0.244	560	0.996
1000	8.45	0.931	0.242	535	1.000
$a_1 = 25.8$; $n_1 = 0.510$; $q = 3.00$					

For some channels and in some range of WIMP masses, we observed that this dependence was given by a simple power law. In fact, for a given channel (i) and a generic mass-dependent $\mathcal{P}$ parameter, a simple power-law scaling behavior would correspond to an expression like

$$\mathcal{P}^{(i)}(M) = m_{\mathcal{P}^{(i)}} M^{n_{\mathcal{P}^{(i)}}}, \tag{10}$$

with $m_{\mathcal{P}^{(i)}}$ and $n_{\mathcal{P}^{(i)}}$ constant values to be determined for the different studied channels. Values of $m_{\mathcal{P}^{(i)}}$ and $n_{\mathcal{P}^{(i)}}$ and their range of validity are presented for each studied channel in the following.

A. *W* boson

As commented above, the correct parametrization for the W boson simulations was given by expression (8). For this boson, there are five mass-dependent parameters: b_1, c_1, d_1, p, and j whose values are detailed in Table IV. The mass independent parameters are $a_1 = 25.8$, $n_1 = 0.51$ and $q = 3.00$. The mass range considered for this boson is 100 to 10^5 GeV. In fact, from $M = 1000$ GeV, the photon spectrum does not change. The parameters obtained fit the enegy spectra from $x = 2 \times 10^{-4}$ until the end of the allowed interval. It can be seen that for low masses the spectrum does not end at $x = 1$ but at smaller energies (e.g. $x \simeq 0.78$ for $M = 100$ GeV) and as masses get higher, the energy tail approaches $x = 1$.

TABLE VI. *Z boson*: b_1, c_1, d_1, p, and j parameters corresponding to (8) in the ZZ channel for different WIMP masses. Mass independent parameters in (8) for this channel are presented at the bottom of the table.

WIMP mass (GeV)	b_1	c_1	d_1	p	j
100	10.3	0.498	0.323	7010	0.702
125	9.74	0.612	0.294	4220	0.836
150	9.49	0.675	0.280	3850	0.894
200	9.28	0.734	0.268	3630	0.943
350	9.02	0.800	0.257	3380	0.978
500	8.95	0.813	0.255	3260	0.988
1000	8.91	0.819	0.254	3140	0.997
$a_1 = 25.8$; $n_1 = 0.5$; $q = 3.87$					

Some of these results are presented in Fig. 1 in the Appendix for four WIMP masses: 100, 200, 350, and 1000 GeV. Besides, mass-dependent parameters b_1, c_1, d_1, p, and j were presented in theAppendix in Fig. 2.

Concerning the scaling behavior of these mass-dependent parameters given by expression (10), we obtain that b_1, c_1, and j parameters scale with a simple power law of M at high masses. In fact, b_1 and c_1 parameters follow a two power-law behavior at low masses. For the d_1 parameter, we find that the sum of two power laws covers this high masses interval, whereas a simple power-law at low masses is obeyed. Parameter p scales with two power laws in the whole studied mass interval. These results are shown in Table V.

B. *Z* boson

For the Z boson the correct parametrization is again the one given by expression (8). For this boson there are five mass-dependent parameters: b_1, c_1, d_1, p, and j which are detailed in Table VI. The mass independent parameters are $a_1 = 25.8$, $n_1 = 0.5$, and $q = 3.87$. The studied WIMP mass range for this boson was from 100 to 10^5 GeV. However, above $M = 1000$ GeV the energy spectrum does not change as can be seen from our simulations.

TABLE V. Parameters corresponding to (10) for the W boson. It can be seen that the p parameter follows two different power laws depending on the WIMP mass interval. For the remaining mass-dependent parameters there is a unique power-law behavior in the WIMP mass interval $350 \leq M \leq 1000$.

Parameter	WIMP mass interval (GeV)	Fitting power law(s)
b_1	$100 \leq M \leq 200$	$0.0433M^{0.765} + 46.4M^{-0.382}$
	$200 < M \leq 1000$	$9.29M^{-0.0139}$
c_1	$100 \leq M \leq 200$	$-27M^{-0.240} + 35.0M^{-0.0643} - 16.5$
	$200 < M \leq 1000$	$0.743M^{0.0331}$
d_1	$100 \leq M \leq 240$	$2.64 \cdot 10^{-4}M^{1.03} + 2.28M^{-0.470}$
	$240 < M \leq 1000$	$0.265M^{-0.0137}$
p	$200 \leq M \leq 1000$	$10^5M^{-1.13} + 285M^{0.0794}$
j	$385 \leq M \leq 1000$	$0.943M^{0.008\,52}$

The chosen parameters values fit the photon spectra from $x = 5 \times 10^{-4}$ until the end of the allowed interval. As for the W case, it can be seen that for low masses the spectrum does not end at $x = 1$ but at smaller energies (e.g. $x \simeq 0.7$ for $M = 100$ GeV) and as masses get higher, the high-energy tail approaches $x = 1$.

Concerning the power-law scaling of the parameters with M, we obtained that parameters b_1, c_1, d_1, and j follow a simple power-law behavior for high WIMP masses. Parameter p follows a two sum power-law behavior for masses higher than 170 GeV. Concerning the d_1 parameter, the whole accessible WIMP mass interval is covered by different either one or two power laws. These results can be seen in Table VII.

C. t quark

For the top, there are six mass-dependent parameters: b_1, n_1, c_2, p q, and l which are detailed in Table VIII. The mass independent parameters are $a_1 = 290$, $c_1 = 1.61$, $d_1 = 0.19$, and $d_2 = 0.845$. The mass range for this quark is from 200 to 10^5 GeV. Nevertheless, from 1000 GeV onwards, the photon spectra do not change as was proven by considering several higher masses. The chosen parameters fit the spectra from $x = 10^{-4}$ until the end of the allowed interval. Again for low masses, the spectra do not end at $x = 1$ but at smaller energies (e.g. $x \simeq 0.7$ for $m = 200$ GeV) and, as masses get higher, the spectral tail approaches $x = 1$.

TABLE IX. Parameters corresponding to (10) for the t quark. It can be seen that all mass-dependent parameters for the t quark follow a simple power-law scaling behavior at intermediate and high WIMP masses. Parameters b_1 and n_1 follow the simple power law for $M > 300$ GeV whereas the rest of the parameters presented do so in the interval $200 \leq M \leq 1000$.

Parameter	WIMP mass interval (GeV)	Fitting power law(s)
b_1	$200 \leq M \leq 350$	$9.32M^{0.0507} + 11.0 \cdot 10^6 M^{-2.91}$
	$350 < M \leq 1000$	$16.4M^{-0.0400}$
n_1	$200 \leq M < 300$	$21.4M^{-0.818} + 0.008\,67M^{0.589}$
	$300 \leq M \leq 1000$	$0.559M^{-0.0379}$
c_2	$200 \leq M \leq 1000$	$8910M^{-3.23}$
p	$200 \leq M < 1000$	$5.78 \times 10^{-5} M^{1.89}$
q	$200 \leq M \leq 1000$	$0.133M^{0.488}$
l	$200 \leq M \leq 1000$	$21.9M^{-0.302}$

Some of these results are presented graphically in Fig. 3 (in the Appendix), for four WIMP masses: 200, 250, 500, and 1000 GeV. Also in the Appendix, mass-dependent parameters b_1, n_1, c_2, p, q, and l are plotted in Fig. 4.

Concerning the scaling behavior of the c_2, p, q, and l parameters, they obey a simple power law in the whole accessible WIMP mass range. Nevertheless, for b_1 and c_1 parameters the simple power-law behavior starts from masses bigger than 350 GeV. These results can be seen in Table IX.

TABLE VII. Parameters corresponding to (10) for the Z boson. It can be seen that all mass-dependent parameters for the Z boson follow a simple power-law scaling at intermediate and high masses.

Parameter	WIMP mass interval (GeV)	Fitting power law(s)
b_1	$500 \leq M \leq 1000$	$9.36M^{-0.00\,710}$
c_1	$465 \leq M \leq 1000$	$0.765M^{0.009\,80}$
d_1	$100 \leq M \leq 191$	$0.00\,999M^{0.530} + 21.5M^{-1.01}$
	$191 < M \leq 360$	$2.02 \times 10^{-9} M^{2.56} + 0.491M^{-0.115}$
	$360 < M \leq 1000$	$0.272M^{-0.009\,90}$
p	$170 \leq M \leq 1000$	$8550M^{-0.166} + 0.476M^{0.984}$
j	$350 \leq M \leq 1000$	$0.884M^{0.0175}$

TABLE VIII. *t quark*: b_1, n_1, c_2, p, q, and l parameters corresponding to (9) in the $t\bar{t}$ channel for different WIMP masses. Mass independent parameters in (9) for this channel are presented at the bottom of the table.

WIMP mass (GeV)	b_1	n_1	c_2	p	q	l
200	14.4	0.477	3.34×10^{-4}	1.34	1.76	4.42
250	13.5	0.457	1.54×10^{-4}	1.95	1.96	4.14
350	13.0	0.448	5.99×10^{-5}	3.78	2.32	3.74
500	12.8	0.442	1.69×10^{-5}	7.40	2.75	3.36
1000	12.4	0.436	1.80×10^{-6}	30.0	3.85	2.72
$a_1 = 290$; $c_1 = 1.61$; $d_1 = 0.19$; $d_2 = 0.845$						

TABLE X. τ *lepton*: n_1 and p parameters corresponding to (6) in the $\tau^+\tau^-$ channel for different WIMP masses. Mass independent parameters in (6) for this channel are presented at the bottom of the table.

WIMP mass (GeV)	n_1	p
25	10.1	221
50	10.0	767
100	9.91	2520
200	9.80	8660
500	9.67	4.01×10^4
1000	9.57	1.35×10^5
10^4	9.25	4.80×10^6
$5 \cdot 10^4$	9.14	5.44×10^7

$a_1 = 14.7$; $b_1 = 5.40$; $b_2 = 5.31$; $n_2 = 1.40$; $c_1 = 2.54$; $d_1 = 0.295$; $c_2 = 0.373$; $d_2 = 0.470$; $q = 0.002\,60$

D. Leptons and quarks

For the rest of the quarks and leptons, the parametrization given in (6) is completely valid. Now we present results for τ and μ leptons and all quarks except for the top.

1. τ lepton

For the τ lepton, there are only two mass-dependent parameters in the spectra fitting function (6): n_1 and p. The remaining parameters are mass independent for this particle and their values are $a_1 = 14.7$, $b_1 = 5.40$, $b_2 = 5.31$, $n_2 = 1.40$, $c_1 = 2.54$, $d_1 = 0.295$, $c_2 = 0.373$, $d_2 = 0.470$, and $q = 0.00260$. These results are presented in Table X.

In this case, the WIMP mass interval considered ranges from 25 to 5×10^4 GeV. For masses higher than 5×10^4 GeV, the spectra do not seem to change, within the statistical uncertainties, with respect to that corresponding to 5×10^4 GeV.

The n_1 parameter scales with the WIMP mass as a simple power law for $M < 5 \times 10^4$ GeV. For the other mass-dependent p parameter, the power-law behavior is valid in two separated intervals with an inflection point in the behavior at $M = 1000$ GeV. These results can be seen in Table XI.

Some of these results are presented graphically in Fig. 5 (in the Appendix), for four WIMP masses: 25, 100, 1000, and 5×10^4 GeV. Also in the Appendix, mass-dependent parameters n_1 and p are presented in Fig. 6.

TABLE XII. μ *lepton*: Parameters corresponding to (7) for different WIMP masses. All parameters in expression (7) are WIMP mass dependent.

WIMP mass (GeV)	p	q	l
25	9510	3.37×10^{-3}	0.787
50	23600	3.40×10^{-3}	0.642
100	54600	3.45×10^{-3}	0.579
200	1.12×10^5	3.50×10^{-3}	0.548
500	2.54×10^5	3.61×10^{-3}	0.523
1000	4.13×10^5	3.70×10^{-3}	0.511
5000	1.18×10^6	3.91×10^{-3}	0.484
10^4	1.84×10^6	4.00×10^{-3}	0.474
5×10^4	5.29×10^6	4.23×10^{-3}	0.454

For this particle, it is worth mentioning the increasing contribution of the logarithmic term in (6) as the WIMP mass increases. This fact can be seen in the presented plots from $x = 0.5$ onwards. As a consequence, the values of the p parameter increase as the WIMP masses increase.

2. μ lepton

For the μ particle and according to expression (7), there are only three mass-dependent parameters: q, p and l. These values are presented in Table XII. In this case, the considered range for WIMP masses is from 25 to 5×10^4 GeV.

The scaling of the p parameter with the WIMP mass shows two well differentiated regimes, with different asymptotic power laws: one from $M = 25$ GeV to $M = 100$ GeV, and another from $M = 750$ GeV to $M = 5 \times 10^4$ GeV. On the other hand, q and l parameters present a sum of two power laws. These results are presented in Table XIII.

As for the τ lepton, the flux of photons increases as the WIMP mass increases. In this case, the q parameter increases as the WIMP masses do so, instead of the p parameter as was the case for the τ.

3. u quark

The mass independent parameters are $a_1 = 5.58$, $b_2 = 5.50$, $c_1 = 0.315$, $c_2 = 0.0$ (therefore d_2 is irrelevant) and $q = 9.30 \times 10^{-4}$. The mass-dependent parameters are b_1, n_1, n_2, d_1, and p. These results are presented in Table XIV.

TABLE XI. Parameters for expression (10) for the τ lepton. It can be seen that n_1 and p parameters follow power-law behaviors.

Parameter	WIMP mass interval (GeV)	Fitting power law(s)
n_1	$25 \leq M < 10^4$	$10.6M^{-0.0148}$
	$10^4 \leq M \leq 5 \times 10^4$	$-7.00M^{-1.99} + 179M^{-0.763} + 9.09$
p	$25 \leq M < 1000$	$0.773M^{1.75}$
	$1000 \leq M \leq 5 \times 10^4$	$3.07M^{1.55}$

TABLE XIII. Parameters for expression (10) for the μ lepton. It can be seen that the p parameter follows simple power laws in two different WIMP mass regimes. Nevertheless, for the q and l parameters a sum of two power laws accounts for the WIMP mass dependence in the whole studied WIMP mass interval.

Parameter	WIMP mass interval (GeV)	Fitting power law(s)
p	$25 \leq M \leq 100$	$176M^{1.25}$
	$750 \leq M \leq 5 \times 10^4$	$4530M^{0.653}$
q	$25 \leq M < 5 \times 10^4$	$0.00230M^{-0.911} + 0.00291M^{0.0348}$
l	$25 \leq M < 5 \times 10^4$	$0.626M^{-0.0300} + 16.4M^{-1.34}$

The analyzed mass range for this quark is from 50 to 8000 GeV.

The spectra of the two highest studied masses (5000 and 8000 GeV) clearly differ in the low energy interval. Therefore, no conclusion can be made about the existence of an asymptotic high masses limit in the spectral shapes. Concerning the mass evolution of the parameters for this quark, we observe simple power-law behaviors for both b_1 and p parameters in the whole studied WIMP mass range interval. On the other hand, n_1, n_2, and d_1 parameters are fitted by a sum of two power laws in the studied range. These results can be seen in Table XV. The chosen values for the parameters turn out to fit the spectra from $x = 5 \times 10^{-4}$ until the end of the allowed energy interval. Nevertheless, for some masses, the fit also applies for lower energies, i.e., lower x values, up to 10^{-4}.

4. d quark

For this channel there are five mass-dependent parameters: b_1, n_1 n_2, c_1, and p. The mass independent parameters are $a_1 = 5.20$, $b_2 = 5.10$, $d_1 = 0.410$, $c_2 = 0.0260$, $d_2 = 0.570$, and $q = 1.40 \times 10^{-4}$. All parameters in this case are presented in Table XVI. The mass range studied for this quark was from 50 to 5000 GeV.

In this channel, no conclusion can be drawn about the existence of an asymptotic high mass limit in the spectral shape. The chosen parameters provide good fits from $x = 2 \times 10^{-3}$ for $M = 50$ GeV whereas for the rest of masses the fits work very well until $x = 5 \times 10^{-4}$.

The scaling of b_1 with M is given by a simple power-law in the whole mass interval, whereas n_1, n_2, and c_1 follow a sum of two power-law behavior in the whole studied mass. Finally, the p parameter presents a power-law behavior for $M > 50$ GeV. These results can be seen in Table XVII.

5. s quark

For the s quark, there are just four mass-dependent parameters b_1, n_2, d_1, and p. The mass independent parameters for this particle in (6) are $a_1 = 4.83$, $n_1 = 2.03$, $b_2 = 6.50$, $c_1 = 0.335$, $c_2 = 0.0$ (d_2 is irrelevant as for the

TABLE XV. Parameters corresponding to (10) for u quark. b_1 and p parameters follow a simple power-law behavior in the whole studied WIMP mass interval. n_1, n_2 and d_1 parameters follow a sum of two power laws in the whole mass interval.

Parameter	WIMP mass interval (GeV)	Fitting power law(s)
b_1	$50 \leq M \leq 8000$	$2.96M^{0.0506}$
n_1	$50 \leq M \leq 8000$	$2.91M^{-0.351} + 1.90M^{0.0172}$
n_2	$50 \leq M \leq 8000$	$0.0587M^{0.146} + 0.848M^{-0.145}$
d_1	$50 \leq M \leq 8000$	$0.317M^{-0.0300} + 0.403M^{-0.351}$
p	$50 \leq M \leq 8000$	$4.74M^{0.839}$

TABLE XIV. u quark: b_1, n_1, n_2, d_1, and p parameters corresponding to expression (6) when applied to the $u\bar{u}$ channel for different WIMP masses. Mass independent parameters in (6) for this channel are presented at the bottom of the table.

WIMP mass (GeV)	b_1	n_1	n_2	d_1	p
50	3.60	2.77	0.585	0.383	129
100	3.75	2.64	0.551	0.355	225
200	3.88	2.54	0.521	0.332	409
500	4.04	2.44	0.490	0.308	856
1000	4.18	2.40	0.472	0.293	1540
2000	4.34	2.39	0.463	0.281	2800
5000	4.55	2.38	0.450	0.266	6000
8000	4.67	2.34	0.448	0.259	8900

$a_1 = 5.58$; $b_2 = 5.50$; $c_1 = 0.315$; $c_2 = 0.0$; $q = 9.30 \times 10^{-4}$.

TABLE XVI. d quark: b_1, n_1, n_2, c_1, and p parameters corresponding to expression (6) when applied to $d\bar{d}$ channel for different WIMP masses. Mass independent parameters in (6) for this channel are presented at the bottom of the table.

WIMP mass (GeV)	b_1	n_1	n_2	c_1	p
50	4.09	2.69	0.561	0.327	17.7
100	4.24	2.47	0.522	0.293	66.2
200	4.39	2.34	0.480	0.258	166
500	4.56	2.28	0.448	0.228	483
1000	4.75	2.25	0.426	0.212	1270
2000	4.91	2.24	0.409	0.200	3130
5000	5.11	2.23	0.394	0.187	10200

$a_1 = 5.20$; $b_2 = 5.10$; $d_1 = 0.410$; $c_2 = 0.0260$; $d_2 = 0.570$; $q = 1.40 \times 10^{-4}$

TABLE XVII. Parameters corresponding to (10) for the d quark. As can be seen, the b_1 parameter follows a simple power law in the whole accessible mass interval. n_1, n_2, and c_1 parameters follow a sum of two power laws in the whole accessible mass interval. Finally, the p parameter follows a power law for $M > 50$ GeV.

Parameter	WIMP mass interval (GeV)	Fitting power law(s)
b_1	$50 \leq M \leq 5000$	$3.39M^{0.0485}$
n_1	$50 \leq M \leq 5000$	$21.8M^{-0.993} + 2.25M^{-0.001\,13}$
n_2	$50 \leq M \leq 5000$	$0.848M^{-0219} + 0.161M^{0.0573}$
c_1	$50 \leq M \leq 5000$	$0.722M^{-0.270} + 0.0544M^{0.0874}$
p	$50 < M \leq 5000$	$0.168M^{1.29}$

u quark), and $q = 2.40 \times 10^{-4}$. All these parameters are detailed in Table XVIII. The studied mass range for this quark is between 50 and 7000 GeV.

As in the d quark case, no conclusion can be drawn about the existence of an asymptotic high mass limit in the spectral shape. The scaling with M of the parameters for this quark is a simple power law for the b_1 parameter for masses higher than 1000 GeV, the sum of two power laws for n_2 and d_1 parameters in the whole studied WIMP mass, and two power laws for the p parameter: one for masses smaller than 1000 GeV and another for masses higher than 1000 GeV. These results are shown in Table XIX.

6. c quark

As for the d quark, there are five mass-dependent parameters. In this case b_1, n_1, c_1, d_1, and p which are presented in Table XX. The mass independent parameters are $a_1 = 5.58$, $b_2 = 7.9$, $n_2 = 0.686$, $c_2 = 0.0$ (therefore d_2 is irrelevant), and $q = 9.00 \cdot 10^{-4}$.

Likewise the u quark, the studied mass range was from 50 to 8000 GeV and again no conclusion can be made about the existence of an asymptotic high mass limit for the spectral shape. Higher masses simulations would be thus required also in this case.

The scaling of b_1 and n_1 with M shows a simple power-law behavior in the considered range. For c_1 and p, the single power-law evolution is only valid for masses above 200 GeV. Finally, the d_1 parameter follows a sum of two power laws in the studied mass range. These results are shown in Table XXI.

TABLE XVIII. *s quark*: b_1, n_2, d_1, and p parameters corresponding to expression (6) when applied to $s\bar{s}$ channel for different WIMP masses. Mass independent parameters in (6) for this channel are presented at the bottom of the table.

WIMP mass (GeV)	b_1	n_2	d_1	p
50	4.78	0.719	0.367	186
100	5.31	0.669	0.332	409
200	5.43	0.648	0.315	605
500	5.60	0.612	0.290	1180
1000	5.73	0.592	0.276	1980
2000	5.87	0.575	0.263	3320
5000	6.07	0.557	0.249	6500
7000	6.12	0.548	0.244	7570
$a_1 = 4.83$; $n_1 = 2.03$; $b_2 = 6.50$; $c_1 = 0.335$; $c_2 = 0.0$; $q = 2.40 \times 10^{-4}$				

TABLE XIX. Parameters corresponding to (10) for the s quark. As can be seen, the b_1 parameter follows a simple power-law behavior for masses higher than 1000 GeV. The n_2 and d_1 parameters follow the sum of two power laws for the whole studied WIMP mass interval. Finally, the p parameter presents two power laws: one for masses smaller than 1000 GeV and another for masses higher than 1000 GeV.

Parameter	WIMP mass interval (GeV)	Fitting power law(s)
b_1	$M > 1000$	$4.54M^{0.0339}$
n_2	$50 \leq M \leq 7000$	$3.68M^{-1.01} + 0.744M^{-0.0352}$
d_1	$50 \leq M \leq 7000$	$0.621M^{-0.674} + 0.414M^{-0.0588}$
p	$50 \leq M \leq 100$	$4.01M^{0.981}$
	$100 < M \leq 7000$	$12.8M^{0.732}$

TABLE XX. *c quark*: b_1, n_1, c_1, d_1, and p parameters corresponding to expression (6) in the $c\bar{c}$ channel for different WIMP masses. Mass independent parameters in (6) for this channel are presented at the bottom of the table.

WIMP mass (GeV)	b_1	n_1	c_1	d_1	p
50	5.93	2.35	0.239	0.428	210
100	5.48	2.08	0.283	0.374	379
200	4.98	1.86	0.330	0.330	673
500	4.50	1.65	0.378	0.288	1230
1000	4.00	1.50	0.406	0.264	2110
2000	3.70	1.35	0.432	0.245	4050
5000	3.27	1.17	0.470	0.221	8080
8000	3.08	1.11	0.494	0.208	12000
$a_1 = 5.58$; $b_2 = 7.90$; $n_2 = 0.686$; $c_2 = 0.0$; $q = 9.00 \times 10^{-4}$					

TABLE XXI. The parameters corresponding to (10) for the c quark. It can be seen that the mass-dependent parameters follow a power-law behavior for intermediate and high WIMP masses. In particular the d_1 parameter follows a sum of two power-law behavior in he whole accessible WIMP mass range.

Parameter	WIMP mass interval (GeV)	Fitting power law(s)
b_1	$50 \leq M \leq 8000$	$9.90M^{-0.130}$
n_1	$50 \leq M \leq 8000$	$4.14M^{-0.148}$
c_1	$500 \leq M \leq 8000$	$0.210M^{0.0951}$
d_1	$50 \leq M \leq 8000$	$1.50M^{-0.632} + 0.479M^{-0.0942}$
p	$200 < M \leq 8000$	$8.11M^{0.812}$

7. b quark

For the b quark, the required gamma rays spectra parametrization is the one given by expression (6). For this particle, the mass independent parameters are $a_1 = 10.0$, $b_2 = 11.0$, $c_2 = 0.0151$, $d_2 = 0.550$, $q = 2.60 \times 10^{-4}$. The mass-dependent parameters are b_1 n_1, n_2, c_1, d_1, and p. Their values are presented in Table XXII.

The studied mass range is from 50 to 8000 GeV. Unlike previous particles for which the spectra did not change remarkably for very high masses, in the present case no conclusion can be drawn about the existence of an asymptotic high mass limit.

Concerning the scaling behavior of the parameters for this quark, we observe that the behavior depends both on the WIMP mass and on the considered parameter. Thus b_1 and n_1 no longer scale with a single power-law for M higher than 100 GeV. For n_2, two simple power laws can be seen, one from 50 to 1000 GeV (not included) and a second one from 1000 (included) to 8000 GeV. c_1 shows also a power-law behavior but only up to 50 GeV. Finally, both d_1 and p, scale with simple power laws from 500 GeV up. These results are summarized in Table XXIII.

Some of these results are presented graphically in Fig. 7, Appendix A 4 for four WIMP masses: 50, 200, 1000 and 5000 GeV. Also in this Appendix, mass-dependent parameters b_1, n_1, n_2, c_1, d_1 and p are plotted in Fig. 8.

TABLE XXII. b *quark*: b_1, n_1, n_2, c_1, d_1, and p parameters corresponding to expression (6) in the $b\bar{b}$ channel for different WIMP masses. Mass independent parameters in (6) for this channel are presented at the bottom of the table.

WIMP mass (GeV)	b_1	n_1	n_2	c_1	d_1	p
50	19.5	6.48	0.710	0.365	0.393	57.8
100	17.1	5.80	0.695	0.403	0.360	138
200	13.1	5.01	0.680	0.415	0.340	281
500	8.76	4.04	0.660	0.431	0.319	623
1000	6.00	3.36	0.647	0.447	0.305	1030
2000	4.60	2.85	0.640	0.460	0.294	1620
5000	3.00	2.26	0.634	0.479	0.280	2670
8000	2.35	2.00	0.629	0.490	0.274	3790
$a_1 = 10.0$; $b_2 = 11.0$; $c_2 = 0.0151$; $d_2 = 0.550$; $q = 2.60 \times 10^{-4}$						

TABLE XXIII. Parameters corresponding to (10) for the b quark. All mass-dependent parameters for the b quark follow simple power-law scalings at intermediate and high energies. Only n_2 and d_1 parameters follow power-law behaviors at low WIMP masses.

Parameter	WIMP mass interval (GeV)	Fitting power law(s)
b_1	$100 < M \leq 8000$	$152M^{-0.462}$
n_1	$100 < M \leq 8000$	$18.7M^{-0.248}$
n_2	$50 \leq M < 1000$	$0.805M^{-0.0319}$
	$1000 \leq M \leq 8000$	$0.707M^{-0.0129}$
c_1	$50 < M \leq 8000$	$0.328M^{0.0447}$
d_1	$50 \leq M < 600$	$0.474M^{-0.0639} + 37.1M^{-1.87}$
	$600 \leq M \leq 8000$	$0.449M^{-0.0552}$
p	$200 < M \leq 8000$	$11.8M^{0.641}$

VII. NUMERICAL CODES

All the calculations performed in this investigation are available at [23].

At this site, we provide the MATHEMATICA [24] files that contain the fitting expressions (6), (8), and (9) for $x^{1.5}dN_\gamma/dx$ presented in this paper when applied for each studied channel. Let us recall that these parametrizations are valid in the corresponding WIMP masses intervals mentioned in the corresponding sections. Also in these files, the fitting formulas for mass-dependent parameters in each channel are presented.

VIII. CONCLUSIONS

In this work, we have extensively studied the photon spectra coming from WIMP pair annihilation into SM particle-antiparticle pairs for all the phenomenologically relevant channels. The covered WIMP mass range has been optimized for each particular channel taking into account mass thresholds, statistics, and saturation of the Monte Carlo simulation. For instance, for light quarks it was from 50 GeV to 8000 GeV, for leptons it was from 25 GeV to 50 TeV, for gauge bosons from 100 GeV to 1000 GeV, and for t quark from 200 to 1000 GeV. All simulated spectra covered the whole accessible energy interval, from extremely low energetic photons until photons with one half of the available total center of mass energy.

Once the spectra were obtained, analytical expressions were proposed to fit the simulation data. Three different fitting functions appeared to be valid depending on the studied channel: one for light quarks and leptons, another for gauge bosons and finally one for t quark very similar to the latter. Those expressions depended on either WIMP mass-dependent or independent parameters. For WIMP mass independent parameters, their values did nevertheless depend on the considered annihilation channel whereas for WIMP mass-dependent ones, their evolutions with WIMP mass were parametrized from the obtained values by continuous and smooth curves.

It is interesting to make general qualitative analysis on the results found in this work. In particular, in Fig. 9 the total number of photons produced by collision for every channel is plotted. This number grows weaker for lepton channels than for (light) quarks, whereas it is constant for gauge bosons (W and Z) and the top annihilation channel. This is a good check of our fits and remembers the physics we are taking into account: On the one hand, the photons

produced in the internal state radiation depends logarithmically on the energy and this is the logarithmic increase observed for leptons and light quarks (all except the top) annihilation channels. In particular, for quarks, this growth is higher (though still logarithmic) because they are strongly interacting particles. This is a kinematic effect that is explained in terms of hadronization, quarks pairs produce more photons because they do produce more particles. In the string approach to QCD phenomenology, this effect is related to how much energy the string (between the two quarks) has. In the case of W and Z bosons, there is not such a string between the W^+W^- or ZZ pairs. It means the photon spectra at different values of DM mass comes from a boosted photon spectra from a W boson at rest. The only string involved in a W or Z decay is from their hadronic decay channels $Z \rightarrow q\bar{q}$, but regardless of the original DM mass, that string will have an energy equal to m_Z (the case of top quark is similar to the W^+W^- or ZZ, since it decays before it hadronizes).

On the other hand, for the ZZ annihilation channel, as the Z gauge boson is not charged, this channel does not directly produce any photons by bremsstrahlung. This means that all photons come from its decay. Therefore, the number of photons must be constant because the fact of producing more energy simply means it has a higher speed in the center of mass system, but in the rest frame system of the Z, the decay process does not change. The computation of photons coming from the top quark annihilation channel does not allow any variation of the number of photons with the energy. Indeed, the top quark has been forced to decay directly into W gauge boson and b quark, without taking into account possible photons coming from its direct bremsstrahlung, what is a good approximation. In the same way, PYTHIA does not take into account the bremsstrahlung radiation coming from the W boson. Therefore, the situation is identical for the top or the Z boson.

In addition to a better understanding of the different channels for photon production from DM annihilation, the use of these fitting functions found in these analyses can save an important amount of computing time and resources: Monte Carlo simulations do not need to be repeated each time that a particular photon spectrum needs to be known for a given channel and center of mass energy. This fact is particularly important for high-energy photons, whose production rate is very suppressed and would require large computation times and to store big amounts of data. Our research was thus able to present very good statistics for those energies.

By having used extensive PYTHIA Monte Carlo simulation we have been able to obtain relatively simple parametrizations of these spectra and fit the corresponding parameters. As our analysis is model independent, it could be useful, both for theoreticians and experimentalists, interested in the indirect DM detection through gamma rays. Given some theoretical model, and the corresponding velocity averaged annihilation cross sections for the different channels, our formulas make it possible to obtain the expected photon spectrum for each particular theoretical model in a relatively simple way. In this sense, further work is in progress to extend our analysis to other stable particles like positron or neutrinos but these results will be presented elsewhere.

ACKNOWLEDGMENTS

This work has been supported in part by MICINN (Spain) Projects No. FIS 2008-01323 and No. FPA 2008-00592, CAM/UCM 910309, MEC Grant No. BES-2006-12059, DOE Grant No. DE-FG02-94ER40823 and MICINN Consolider-Ingenio MULTIDARK CSD2009-00064. We are particularly grateful to Professor Jonathan Feng for his continuous and encouraging help at UC Irvine during the summer of 2007. We would also like to thank Dr. Mario Bondioli for his preliminary help with simulation software and Dr. Mirco Cannoni, Professor Mario E. Gomez and Professor Mikhail Voloshin for interesting discussions about different aspects of the physical meaning of the spectra behavior. Dr. Abelardo Moralejo drew our attention of some particular aspects of bremsstrahlung. Finally, fruitful discussions were held with Daniel Nieto about detectors' technicalities and improvement of the numerical codes. R. L. acknowledges financial support given by Ministero dell'Istruzione, dell'Università e della Ricerca (MIUR), by the University of Torino (UniTO), by the Istituto Nazionale di Fisica Nucleare (INFN) within the Astroparticle Physics Project, and by the Italian Space Agency (ASI) under Contract No. I/088/06/0. AdlCD wants to thank David Fernández (UCM) for his technical support with the performed simulations and Dr. Javier Almeida for his help to manage simulation results. Scientific discussions about other available simulation software were held with Beatriz Cañadas.

A. APPENDIX

In this section we present simulations for some of the studied channels: W^+W^-, $t\bar{t}$, $\tau^+\tau^-$, and $b\bar{b}$. For these channels four simulated spectra are presented together with the proposed fit formulas, the χ^2 of the fits and the number of degrees of freedom (d.o.f.) calculated as the number of simulated points minus the number of free parameters. We have computed the χ^2 by assuming a constant relative uncertainty of 10% in the data simulated by PYTHIA. This is a conservative approach, since this is below the uncertainty not only on quark fragmentation functions, but also on the difference with other simulation packages (such as HERWIG), or even with other versions of the same PYTHIA. For each channel, the evolution with WIMP mass of mass-dependent parameters has also been plotted. Figure 9 shows the running with the WIMP mass of the total number of photons per WIMP pair annihilation.

1. Plots for W gauge boson

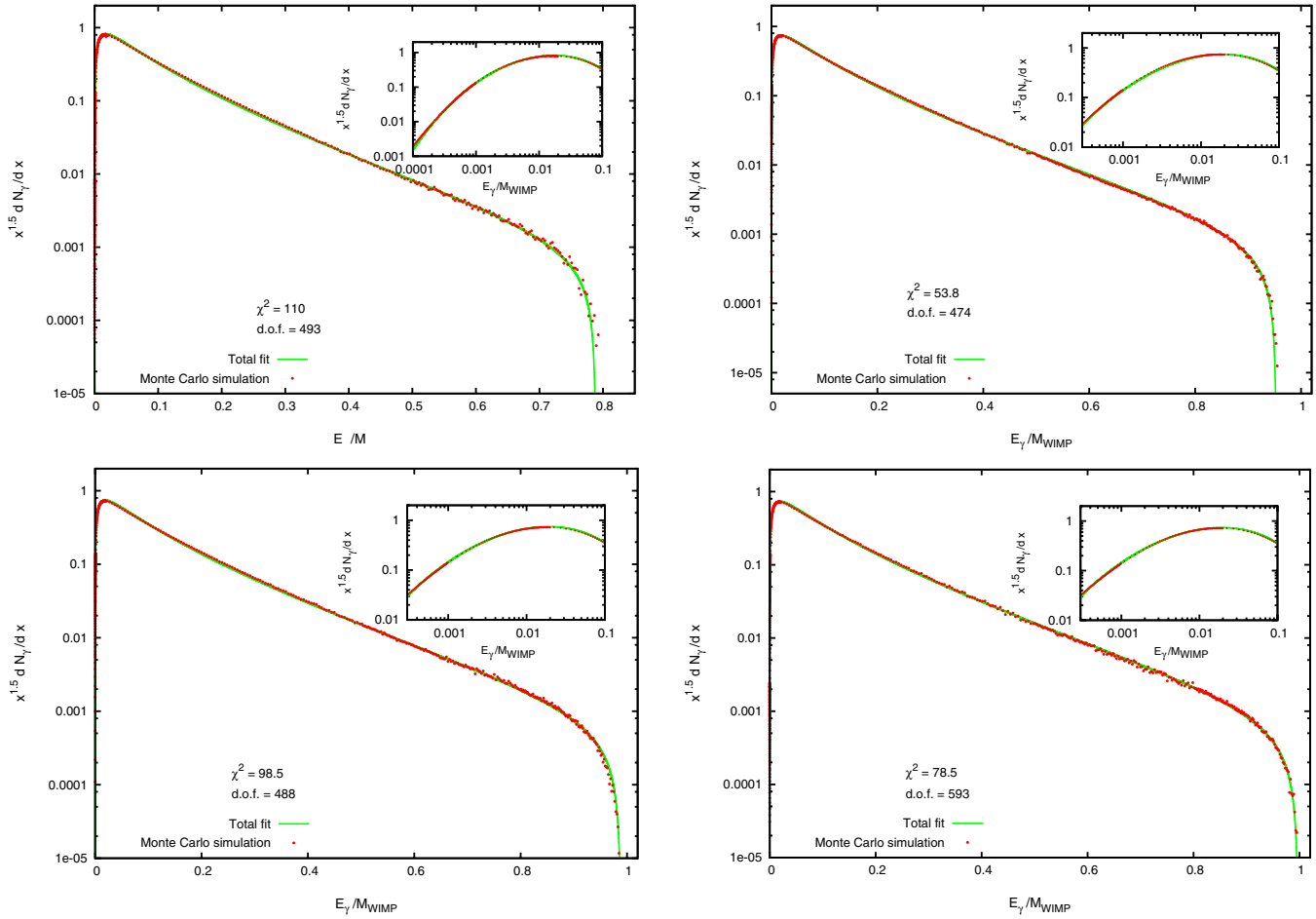

FIG. 1 (color online). Photon spectra for four different WIMP masses (100, 200, 350, and 1000 GeV) in the W^+W^- channel. Red dotted points are PYTHIA simulations and solid lines correspond to the proposed fitting functions. From left to right and from top to bottom, the photon spectra are for $M = 100, 200, 350$, and 1000 GeV, respectively.

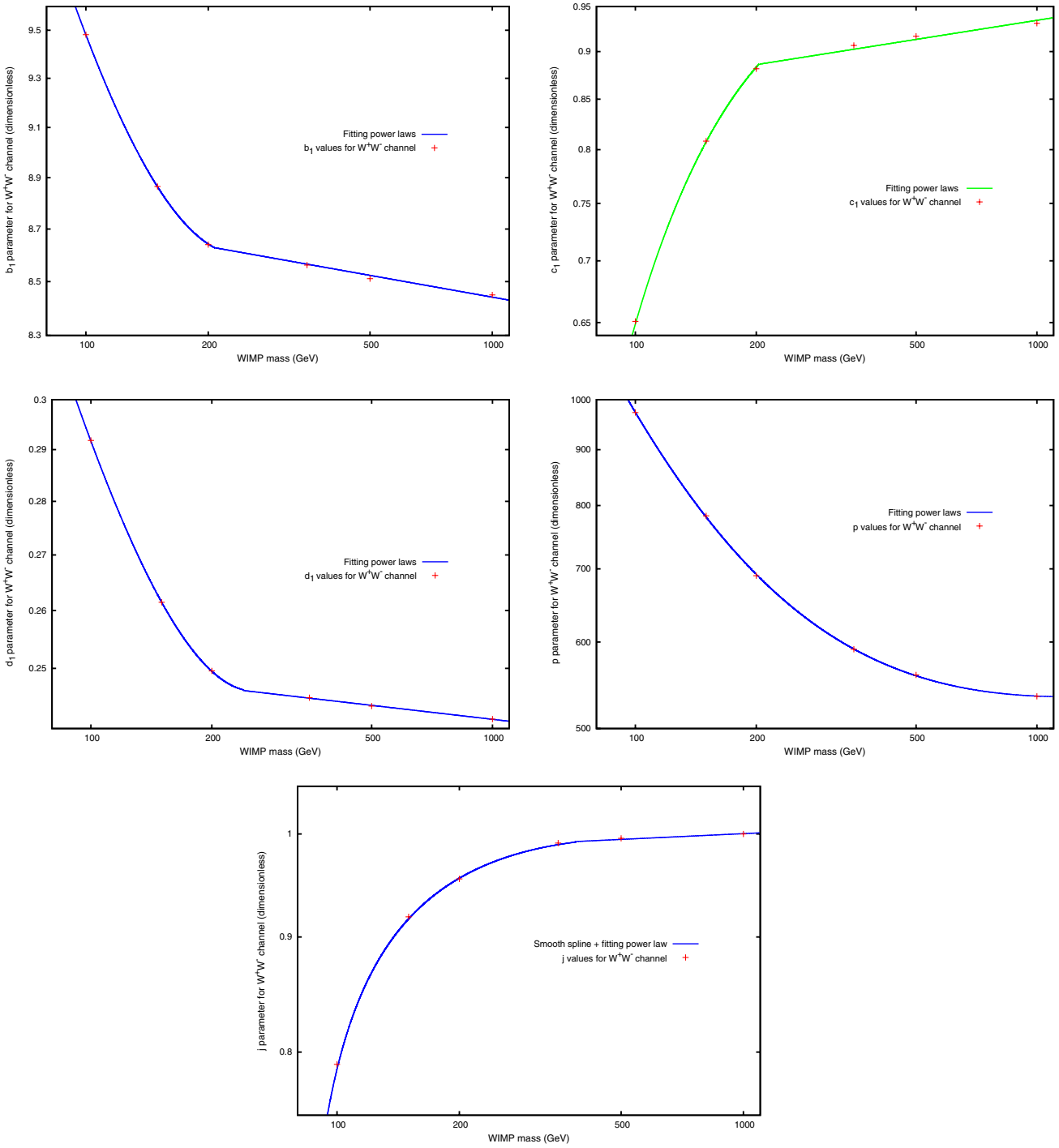

FIG. 2 (color online). From left to right and from top to bottom: mass dependence of the b_1, c_1, d_1, p, and j parameters for W^+W^- channel. Crossed points are the parameters' values found after the fitting process for each WIMP mass and solid lines correspond to the proposed fitting functions. Relative errors of the fitted values range from 1% to 3% for these parameters.

2. Plots for t quark

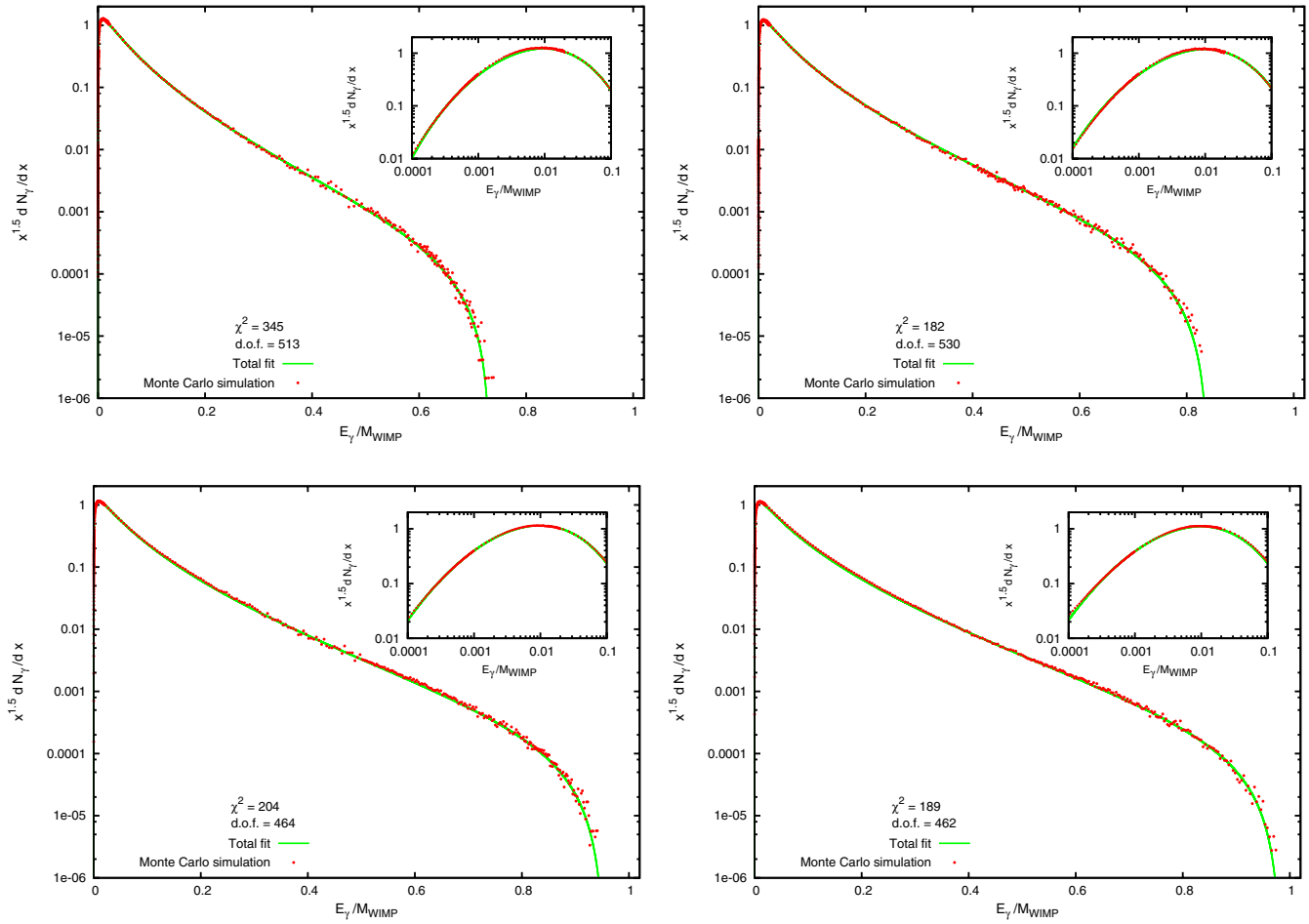

FIG. 3 (color online). Photon spectra for four different WIMP masses (200, 250, 500, and 1000 GeV) in the $t\bar{t}$ annihilation channel. Red dotted points are PYTHIA simulations and solid lines correspond to the proposed fitting functions. From left to right and from top to bottom, the photon spectra are for $M = 200, 250, 500$, and 1000 GeV, respectively.

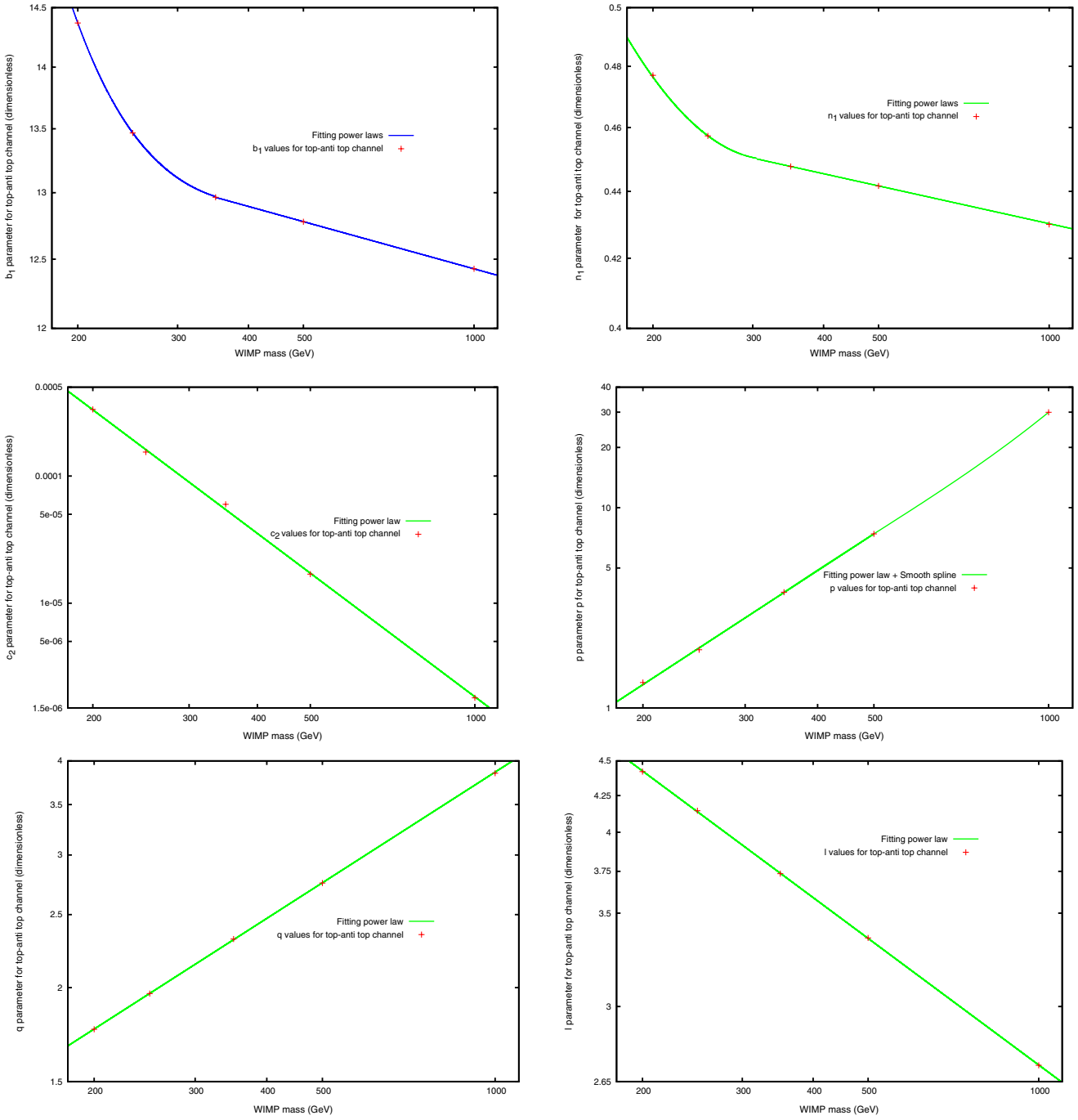

FIG. 4 (color online). From left to right and from top to bottom: mass dependence of b_1, n_1, c_2, p, q, and l parameters for the $t\bar{t}$ annihilation channel. Crossed points are the parameters' values found after the fitting process for each WIMP mass and solid lines correspond to the proposed fitting functions. Relative errors of the fitted values range from 1% to 28% for these parameters.

3. Plots for τ lepton

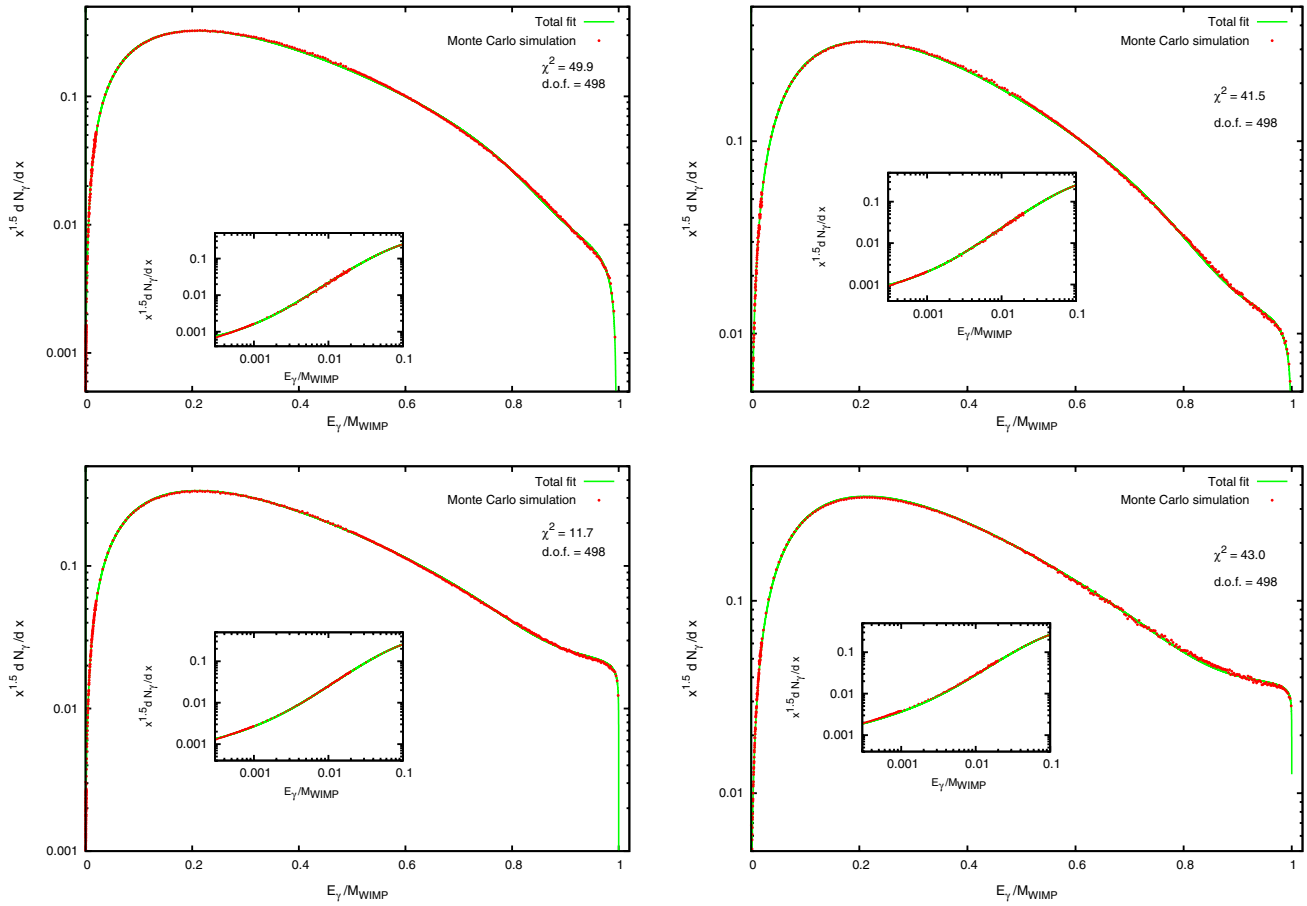

FIG. 5 (color online). Photon spectra for four different WIMP masses (25, 100, 1000, and 5×10^4 GeV) in the $\tau^+\tau^-$ annihilation channel. Red dotted points are PYTHIA simulations and solid lines correspond to the proposed fitting functions. From left to right and from top to bottom, the photon spectra are for $M = 25, 100, 1000$, and 5×10^4 GeV, respectively.

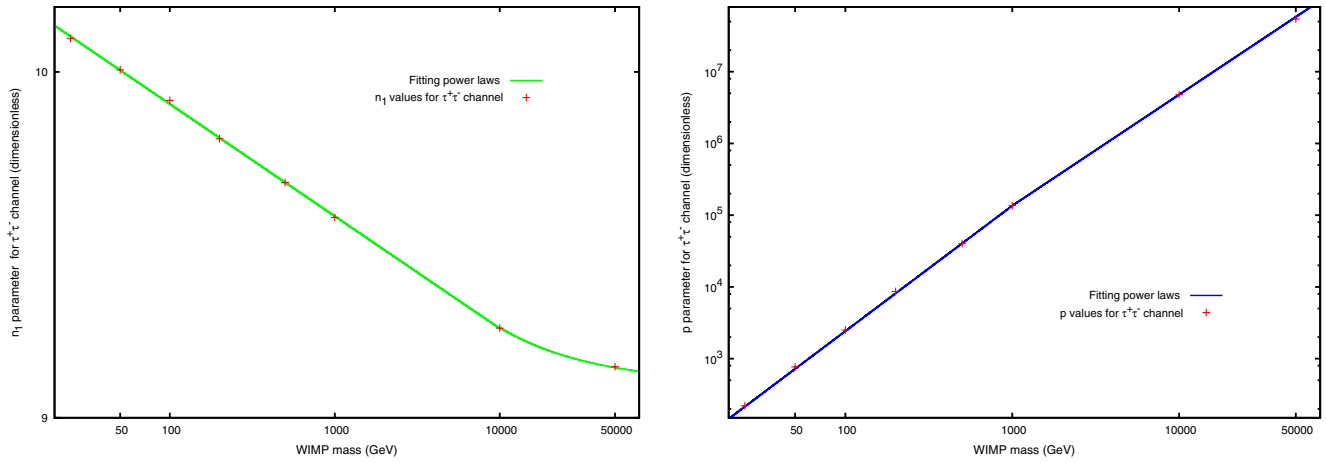

FIG. 6 (color online). From left to right and from top to bottom: mass dependence of the n_1 and p parameters for the $\tau^+\tau^-$ annihilation channel. Crossed points are the parameters' values found after the fitting process for each WIMP mass and solid lines correspond to the proposed fitting functions. Relative errors of the fitted values range from 1% to 6% for these parameters.

4. Plots for b quark

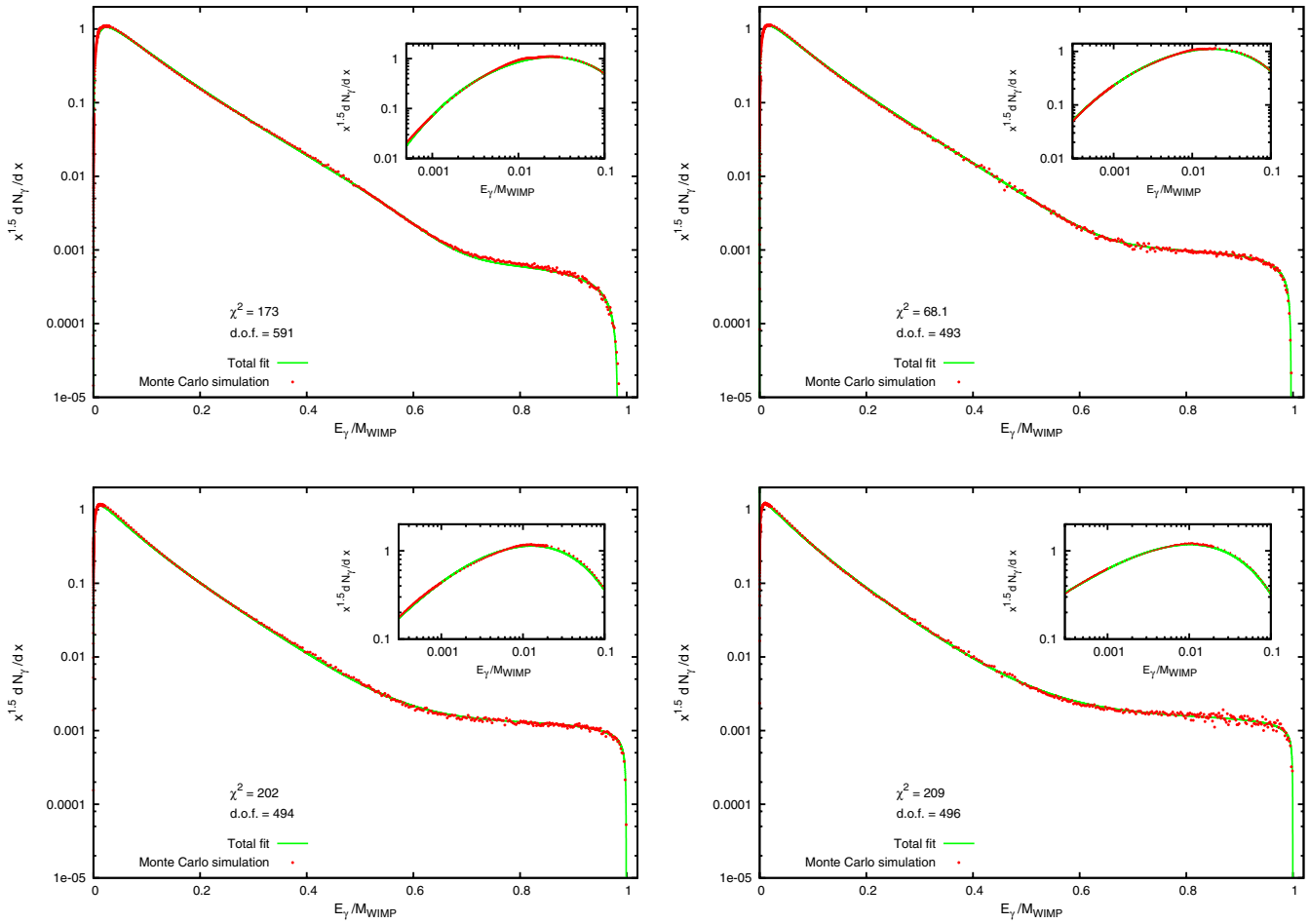

FIG. 7 (color online). Photon spectra for four different WIMP masses (50, 200, 1000, and 5000 GeV) in the $b\bar{b}$ annihilation channel. Red dotted points are PYTHIA simulations and solid lines correspond to the proposed fitting functions. From left to right and from top to bottom, the photon spectra are for $M = 50, 200, 1000$, and 5000 GeV, respectively.

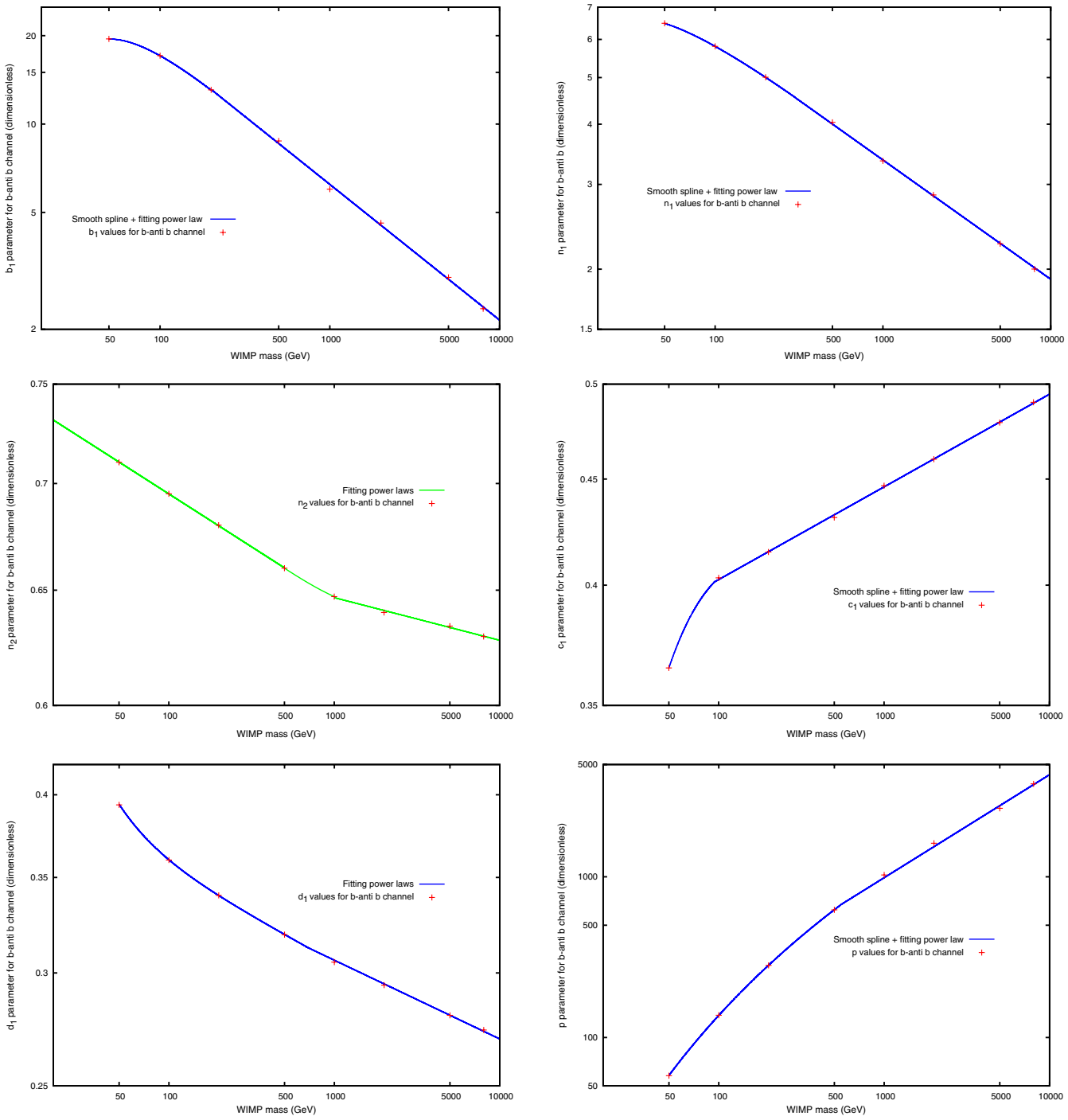

FIG. 8 (color online). From left to right and from top to bottom: mass dependence of the b_1, n_1, n_2, c_1, d_1, and p parameters for the $b\bar{b}$ annihilation channel. Crossed points are the parameters' values found after the fitting process for each WIMP mass and solid lines correspond to the proposed fitting functions. Relative errors of the fitted values range from 1% to 15% for these parameters.

5. Photon number per WIMPs annihilation

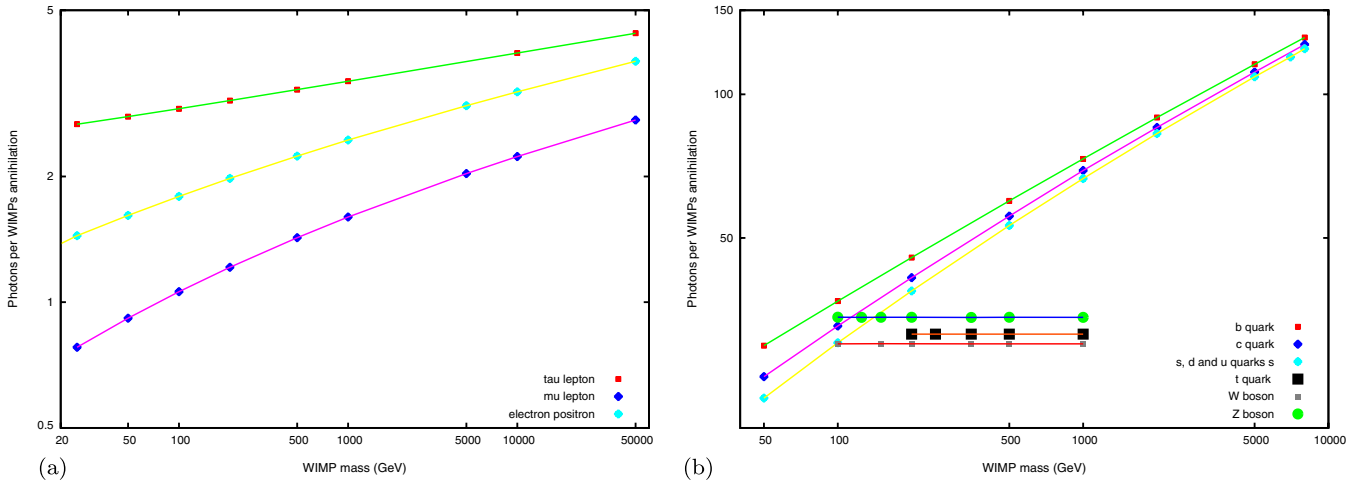

FIG. 9 (color online). Total photon number per WIMP annihilation: On the left (a) the leptonic channels are presented whereas on the right (b) both gauge bosons and quarks results are plotted. The points are the values presented in Tables I, II, and III divided by the number of WIMPs annihilations in each case. The curves are the smooth curves joining the points for every channel.

[1] P. Achard *et al.*, Phys. Lett. B **597**, 145 (2004); S. Heinemeyer *et al.*, ECONF C0508141: PLEN0044, (2005); J. A. R. Cembranos, A. Rajaraman, and F. Takayama, Europhys. Lett. **82**, 21001 (2008); J. A. R. Cembranos, A. Dobado, and A. L. Maroto, Phys. Rev. D **65**, 026005 (2001); **70**, 096001 (2004); **73**, 057303 (2006); J. Phys. A **40**, 6631 (2007); A. Juste *et al.*, arXiv:hep-ph/0601112; J. A. R. Cembranos *et al.*, AIP Conf. Proc. **903**, 591 (2007); ILC Collaboration, arXiv:0709.1893; J. A. R. Cembranos, A. Dobado, and A. L. Maroto, AIP Conf. Proc. **670**, 235 (2003); Int. J. Mod. Phys. D **13**, 2275 (2004); Phys. Rev. D **73**, 035008 (2006); J. A. R. Cembranos, J. H. Montes de Oca Y., and L. Prado, arXiv:1008.4435; J. Alcaraz *et al.*, Phys. Rev. D **67**, 075010 (2003).

[2] L. Covi, J. E. Kim, and L. Roszkowski, Phys. Rev. Lett. **82**, 4180 (1999); J. L. Feng, A. Rajaraman, and F. Takayama, Phys. Rev. Lett. **91**, 011302 (2003); Phys. Rev. D **68**, 063504 (2003); J. A. R. Cembranos, J. L. Feng, A. Rajaraman, and F. Takayama, Phys. Rev. Lett. **95**, 181301 (2005); J. A. R. Cembranos, J. L. Feng, and L. E. Strigari, Phys. Rev. D **75**, 036004 (2007); Phys. Rev. Lett. **99**, 191301 (2007); T. Biswas *et al.*, Phys. Rev. Lett. **104**, 021601 (2010); J. High Energy Phys. 10 (2010) 048; Phys. Rev. D **82**, 085028 (2010); J. A. R. Cembranos, K. A. Olive, M. Peloso, and J. P. Uzan, J. Cosmol. Astropart. Phys. 07 (2009) 025; J. A. R. Cembranos, AIP Conf. Proc. **1182**, 288 (2009).

[3] X. L. Chen and M. Kamionkowski, Phys. Rev. D **70**, 043502 (2004); L. Zhang, X. Chen, M. Kamionkowski, Z. Si, and Z. Zheng, Phys. Rev. D **76**, 061301 (2007); K. Sigurdson and M. Kamionkowski, Phys. Rev. Lett. **92**, 171302 (2004); J. A. R. Cembranos *et al.*, Phys. Rev. Lett. **90**, 241301 (2003); Phys. Rev. D **68**, 103505 (2003); J. Cosmol. Astropart. Phys. 10 (2008) 039; J. A. R. Cembranos and L. E. Strigari, Phys. Rev. D **77**, 123519 (2008); J. A. R. Cembranos, Phys. Rev. D **73**, 064029 (2006); Phys. Rev. Lett. **102**, 141301 (2009); S. Profumo, K. Sigurdson, P. Ullio, and M. Kamionkowski, Phys. Rev. D **71**, 023518 (2005); M. Kaplinghat, Phys. Rev. D **72**, 063510 (2005); L. E. Strigari, M. Kaplinghat, and J. S. Bullock, Phys. Rev. D **75**, 061303 (2007).

[4] L. Bergstrom, P. Ullio, and J. H. Buckley, Astropart. Phys. **9**, 137 (1998).

[5] J. L. Feng, K. T. Matchev, and F. Wilczek, Phys. Rev. D **63**, 045024 (2001).

[6] N. Fornengo, L. Pieri, and S. Scopel, Phys. Rev. D **70**, 103529 (2004).

[7] E. Komatsu *et al.*, Astrophys. J. Suppl. Ser. **192**, 18 (2011).

[8] W. J. Percival *et al.*, Mon. Not. R. Astron. Soc. **401**, 2148 (2010).

[9] A. G. Riess *et al.*, Astrophys. J. **699**, 539 (2009).

[10] L. Bergstrom, T. Bringmann, M. Eriksson, and M. Gustafsson, Phys. Rev. Lett. **94**, 131301 (2005); A. Birkedal, K. T. Matchev, M. Perelstein *et al.*, arXiv:hep-ph/0507194; L. Bergstrom, T. Bringmann, M. Eriksson, and M. Gustafsson, Phys. Rev. Lett. **95**, 241301 (2005); F. Aharonian *et al.* (H.E.S.S. Collaboration), Phys. Rev. Lett. **97**, 221102 (2006); **97**, 249901 (2006); D. Horns (H.E.S.S Collaboration), Adv. Space Res. **41**, 2024 (2008).

[11] P. Ciafaloni, D. Comelli, A. Riotto *et al.*, arXiv:1009.0224.
[12] F. Stoehr, S. D. White, V. Springel, G. Tormen, and N. Yoshida, Mon. Not. R. Astron. Soc. **345**, 1313 (2003).
[13] V. Debattista and J. A. Sellwood, Astrophys. J. **493**, L5 (1998); J. J. Binney and N. W. Evans, Mon. Not. R. Astron. Soc. **327**, L27 (2001); N. W. Evans, in *IDM 2000: The Third International Conference on the Identification of Dark Matter*, edited by N. Spooner and V. Kudraytsev (World Scientific, Singapore, 2001), p. 85; F. Donato, G. Gentile, P. Salucci *et al.*, arXiv:0904.4054 [Mon. Not. Roy. Astron. Soc. (to be published)]; P. Salucci, A. Lapi, C. Tonini *et al.*, Mon. Not. R. Astron. Soc. **378**, 41 (2007).
[14] N. W. Evans, F. Ferrer, and S. Sarkar, Phys. Rev. D **69**, 123501 (2004); J. D. Simon *et al.*, arXiv:1007.4198; R. Essig, N. Sehgal, L. E. Strigari, M. Geha, and J. D. Simon, Phys. Rev. D **82**, 123503 (2010); M. Perelstein and B. Shakya, J. Cosmol. Astropart. Phys. 10 (2010) 016.
[15] A. Pinzke, C. Pfrommer, and L. Bergstrom, Phys. Rev. Lett. **103**, 181302 (2009); T. E. Jeltema, J. Kehayias, and S. Profumo, Phys. Rev. D **80**, 023005 (2009).
[16] A. Tasitsiomiu, J. Gaskins, and A. V. Olinto, Astropart. Phys. **21**, 637 (2004).
[17] R. Rando (FERMI LAT Collaboration), arXiv:0907.0626.
[18] AMS Collaboration, Report No. 2003-08-02; J. A. R. Cembranos, A. Dobado, and A. L. Maroto, arXiv:astro-ph/0611911.
[19] T. Sjostrand, S. Mrenna, and P. Skands, J. High Energy Phys. 05 (2006) 026.
[20] T. Bringmann, L. Bergstrom, and J. Edsjo, J. High Energy Phys. 01 (2008) 049.
[21] M. Cannoni, M. E. Gomez, M. A. Sanchez-Conde, F. Prada, and O. Panella, Phys. Rev. D **81**, 107303 (2010).
[22] D. Hooper and J. March-Russell, Phys. Lett. B **608**, 17 (2005).
[23] http://teorica.fis.ucm.es/~PaginaWeb/downloads.html.
[24] S. Wolfram, *MATHEMATICA: A System for Doing Mathematics by Computer* (Addison-Wesley, New York, 1991).